Chall. Nano Micro Scale Sci. Tech., 10(2): 19-32, Summer and Autumn 2022
DOI: 10.22111/cnmst.2024.44828.1233

ORIGINAL RESEARCH PAPER

Free Vibrations Analysis of Cracked Micro Cantilever Beams Based on the Modified Strain Gradient Theory

Abbas Rahi [1*], Behzad Heidarpour[2]

1 Associate Professor, Faculty of Mechanical and Energy Engineering, Shahid Beheshti University, Tehran, Iran*
2 Ph.D. Candidate, Faculty of Mechanical and Energy Engineering, Shahid Beheshti University, Tehran, Iran

ABSTRACT: This paper explores the lateral vibration behavior of a micro cantilever beam with an open edge crack under axial load using the modified strain gradient theory (MSGT). A concentrated mass, incorporating its rotational inertia, is positioned at the beam's free end. The open edge crack is represented using the Dirac delta function. By employing MSGT, Hamilton's principle, and the Dirac delta function, the governing equations for system motion and relevant boundary conditions are derived to examine the size-dependence effects. Analytical solutions for the first and second natural frequencies of the cracked cantilever beam are provided, validated through finite element modeling. The study further investigates the impact of various system parameters, including material length scale parameters, crack depth, crack location, cantilever beam length, axial load, and the presence of the concentrated mass, on the natural frequencies. The findings demonstrate that the crack depth, crack location, and material length scale parameters considerably influence the lateral vibration characteristics of the system. Notably, increasing the values of l_i/h from 0 to 0.25 leads to an approximate 40% rise in the natural frequency.

KEYWORDS*: Micro cantilever beam; Open edge crack; MSGT; Size dependency; lateral vibrations; Axial load*

INTRODUCTION

Micro beams are one of the most commonly importance elements which are used in field of the micro-electro-mechanical systems (MEMS) such as sensors (Pei et al., 2004 [1]; Lun et al., 2006 [2]; McMahan et al., 2004, [3]), micro switches (Hua et al., 2007, [4]; Coutu et al., 2004, [5]), micro actuators (Rezazadeh et al., 2006 [6]; Moghimi-Zand and Ahmadian, 2009 [7]; Hu et al., 2004 [8]; Mojahedi et al., 2010 [9]; Abdel-Rahman et al., 2002 [10]), and atomic force microscopes (Mahdavi et al., 2008 [11]; Chang et al., 2008 [12]; Turner and Wiehn, 2001 [13]; Lee and Chang, 2008 [14]). Several researchers show that the classical continuum mechanics theory is incapable of explanation and prediction of the static and dynamic behaviors of small size structures such as micro beams (Lam and Chong, 1999 [15]; Fleck et al., 1994 [16]; lam et al., 2003 [17]; Chong and Lam, 1999 [18]). In other words, the important subject in the study of mechanical behaviors of the micro structures which are used in the micro devices is consideration of the size dependency.

In recent years, to capture of the size dependency in the mechanical behaviors of micro size structures, some non-classical continuum theories such as nonlocal elasticity theory, couple stress theory, strain gradient theory, and surface elasticity theory have been presented by investigators (Eringen, 1972 [19]; Mindlin and Tiersten, 1962 [20]; Yang et al., 2002 [21]; Lam et al., 2003 [17]; Gurtin and Murdoch, 1978 [22]).

The couple stress theory offered by Mindlin and Tiersten, 1962 [20] as a non-classical continuum theory to consider the size dependency effect with using from two material length scale parameters. Then, Yang et al., 2002 [21] suggested the modified couple stress theory (MCST) based on using one material length scale parameter to capture the size effect.

Mindlin, 1965 [23] and Mindlin and Eshel (1968) [24] presented a higher-order continuum of the strain gradient elasticity theory by using the first and second gradients of the strain to consider the size effect in small scale structures. Fleck and Hutchinson (1993) [25] reformulated the Mindlin's theory and called it the strain gradient theory (SGT). After that, the modified strain gradient theory (MSGT) proposed by Lam et al. (2003) [17], to consider the size dependency in materials mechanical behavior using three constants of material length scale parameters. It is noted that the MCST is a special case of the MSGT which can be obtained by letting two first constants of material length scale parameters in the MSGT to equal zero. Park and Gao, 2006 [26]; Ma et al., 2008 [27]; Liang et al., 2015 [28]; Asghari et al., 2011 [29]; Ghiasi, 2016 [30]; and Dai et al., 2015 [31] studied static or dynamic behaviors of Micro/Nano beams based on the MCST to capture the size dependency. Also, several researchers such as Şimşek et al., 2017 [32]; Askari and Tahani, 2017 [33]; Alinaghizadeh et al., 2017 [34]; Guo et al., 2017 [35]; and He et al., 2017 [36] investigated mechanical behaviors of micro plates based on the MCST.

* Corresponding author's email: a_rahi@sbu.ac.ir
Tel.: +989372737526

Inasmuch, The SGT or the MSGT have been also employed as a fundamental formulation to consider the size effect in mechanical behaviors of micro beams (Vatankhah et al., 2013 [37]; Kahrobaiyan et al., 2011 [38]; Kahrobaiyan et al., 2013 [39]; Joseph et al., 2017 [40]; Ansari et al., 2016 [41]), and microplates (Mirsalehi et al., 2016 [42]; Ansari et al., 2014 [43]).

In the other hand, limited numbers of investigators studied the vibrational behaviors of cracked micro beams. Micro beams are susceptible to cracks and defects due to factors such as initial material imperfections, fabrication processes, fatigue, and stress concentration. When a crack occurs, it leads to a reduction in local stiffness within the beam. As a consequence, the vibration characteristics, bending behavior, and overall performance of the structure undergo significant changes. Consequently, the investigation of cracked structures has emerged as a highly important area of research.

Several researchers have made notable contributions to the understanding of cracked micro structures. For instance, Loya et al. (2009) [44] and Tadi Beni et al. (2015) [45] focused on exploring the transverse vibrations of cracked nano-beams. Loya et al. employed a linear torsion spring based on the nonlocal elasticity theory, while Tadi Beni et al. utilized the modified couple stress theory. Hasheminejad et al. (2011) [46] and Wang and Baolin Wang (2013) [47] conducted studies on the lateral vibrations of cracked nano-beams, incorporating surface effects modeling and surface energy theory, respectively. They also employed a linear torsion spring to model the crack. Torabi and Nafar Dastgerdi (2012) [48] investigated the vibration analysis of cracked nano-beams using Eringen's nonlocal elasticity model and Timoshenko beam theory, employing a torsion spring model. Furthermore, Liu et al. (2013) [49] explored the vibration response of cracked micro cantilever beams, considering the influence of electrostatic force through a concentrated torsion spring. Akbas (2017) [50], using the finite element method, investigated the vibrations behavior of open-edge cracked FGM cantilever micro beams based on the Mass Conserving Spring Theory (MCST). Khorshidi (2017) [51] delved into the buckling behavior of cracked nano-beams, utilizing the nonlocal elasticity theory and employing a torsion spring model for the crack. Esen et al. (2021) [52] investigated the vibrational behavior of a functionally graded (FG) cracked microbeam placed on an elastic base and subjected to thermal and magnetic fields. They modeled the crack as a rotating spring and connected two parts of the microbeam at the crack position. Also, they used the theory of non-local elasticity in order to apply the size effect. The results of their study show that the presence of cracks reduces the frequency of the system. Hossein Darban et al. (2022) [53] formulated a non-local model to study the size-dependent free transverse vibrations of nanobeams with arbitrary number of cracks. They modeled the crack effect by creating a discontinuity in slope and transverse displacement in the cracked section, proportional to the bending moment and the shear force transferred from it. They defined the kinematic field based on the Bernoulli-Euler beam theory and considered the small size effect using the constitutive equation of the stress-based non-local tension theory.

The crack was modeled using a massless elastic torsion spring, adhering to the classical cracked-beam theory.

By extensively studying the lateral vibration behavior of cracked micro cantilever beams, we can uncover numerous practical applications and implications. Some notable aspects include:

- Advancing Engineering Solutions: Understanding the lateral vibration behavior of cracked micro cantilever beams is pivotal in optimizing the design and performance of microelectromechanical systems (MEMS), nanotechnology applications, and sensor devices. This research aids in improving the reliability, efficiency, and functionality of these systems.
- Enhanced Device Performance: Cracks significantly impact the performance of micro cantilever beams. Analyzing their lateral vibration behavior provides valuable knowledge for predicting and mitigating performance degradation. It enables engineers to optimize the dynamic response, stability, and durability of micro-scale devices.
- Building on Existing Research: The collective works of researchers mentioned above form the foundation for further exploration. By expanding on the existing research, we can deepen our understanding of crack-related phenomena, develop more accurate models, and refine methodologies for predicting and analyzing the lateral vibration behavior of micro-scale structures.

In summary, studying the lateral vibration behavior of cracked micro cantilever beams holds great significance for practical applications, structural analysis, and advancing scientific knowledge. The findings from these investigations contribute to the development of robust micro-scale systems, ensuring their reliability, safety, and superior performance.

In the present study, lateral vibrations behavior of a cracked micro cantilever beam with an open edge crack and subjected to an axial load is investigated based on the MSGT. The crack is modeled by Dirac delta function to the reduction of the local stiffness of the micro beam in the location of the crack. The governing equations of motion and the associated boundary conditions are obtained based on the MSGT and using Hamilton's principle and Dirac delta function. Then, to obtain analytically of natural frequencies of the system, the assumed modes method is used to transform the governing equations into a set of infinite ordinary differential equations. Finally, variation of first and second natural frequencies of the cracked micro cantilever beam are investigated with respect to the different values of the system parameters such as crack depth, crack location, length of the micro cantilever beam, material length scale parameters l_0, l_1, l_2, axial load, concentrated mass and its rotary inertia values based on the MSGT.

Theory and Mathematical Formulation

Modeling of the System

Figure 1 shows a schematic view of a cracked micro cantilever elastic beam subjected to an axial load. The concentrated mass M, with mass moment of inertia I_M, is mounted on end free of the micro beam. The micro elastic beam has width b, height h, length L, cross section A, density ρ, and second moment of cross-section area I_b. Also, the open edge crack with depth a which located at a distance L_c from the left end, the coordinate system X-Y-Z, the axial load P, and the concentrated mass M, have been shown in Fig. 1

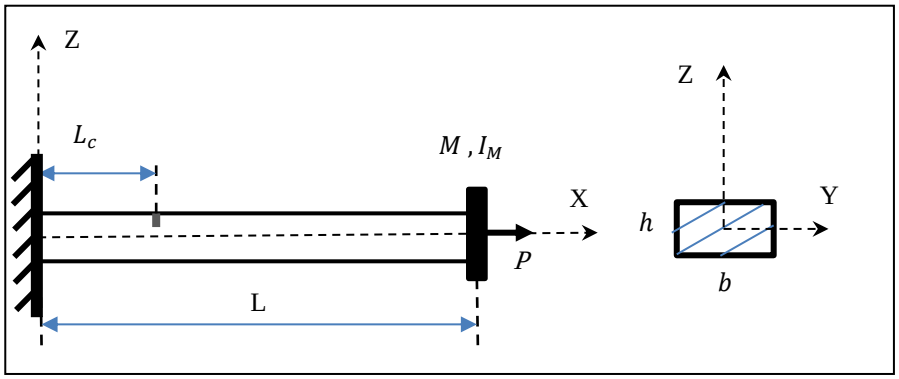

Fig. 1. Modeling of a cracked micro cantilever beam subjected to an axial load $\boldsymbol{P}$ with an open edge crack at location $\boldsymbol{L_c}$

The Modified Strain Gradient Theory

To overcome the limitations of classical continuum theories, size-dependent continuum theories have been developed and applied to analyze microstructures. These include nonlocal elasticity, modified nonlocal elasticity, couple stress, modified couple stress, surface elasticity, and strain gradient. The nonlocal elasticity theory leads to stiffness-softening mechanisms, while the strain gradient elasticity theory results in stiffness hardening.

One well-known theory proposed by Mindlin, which considers all components of higher-order deformation, is widely used in microstructure studies. However, its application in engineering practices is challenging due to its reliance on five MLSPs.

To address this difficulty, Lam et al. proposed the modified strain gradient theory by reducing two MLSPs. This theory, based on the symmetric condition of the couple-stress tensor equilibrium equation, has been utilized in several studies involving micro/nanobeams and micro/nanoplates (Thai et al., 2020 [54]). Based on the modified strain gradient theory, the strain energy density of an isotropic elastic material can be obtained as follows (Lam et al., 2003 [17])

$$\pi_0 = \frac{1}{2}\sigma_{ij}\varepsilon_{ij} + \frac{1}{2}p_i\,\gamma_i + \frac{1}{2}\tau^{(1)}_{ijk}\,\eta^{(1)}_{ijk} + \frac{1}{2}m^s_{ij}\,\chi^s_{ij} \tag{1}$$

where

$$\varepsilon_{ij} = \frac{1}{2}\left(u_{i,j} + u_{j,i}\right) \tag{2}$$

$$\gamma_i = \varepsilon_{mm,i} \tag{3}$$

$$\eta^{(1)}_{ijk} = \frac{1}{3}\left(\varepsilon_{ij,k} + \varepsilon_{jk,i} + \varepsilon_{ki,j}\right) - \frac{1}{15}\,\delta_{ij}\left(\varepsilon_{mm,k} + 2\varepsilon_{mk,m}\right) - \frac{1}{15}\left[\delta_{jk}\left(\varepsilon_{mm,i} + 2\varepsilon_{mi,m}\right) + \delta_{ki}\left(\varepsilon_{mm,j} + 2\varepsilon_{mj,m}\right)\right] \tag{4}$$

$$\chi^s_{ij} = \frac{1}{2}\left(\theta_{i,j} + \theta_{j,i}\right) \tag{5}$$

$$\theta_i = \frac{1}{2}\epsilon_{ijk}\,u_{k,j} \tag{6}$$

where ε_{ij} is components of the strain tensor, γ_i is components of the dilatation gradient vector, $\eta^{(1)}_{ijk}$ is components of the deviatoric stretch gradient tensor, χ^s_{ij} is symmetric part of the rotation gradient tensor, u_i is components of the displacement vector, θ_i is components of the infinitesimal rotation vector, and ϵ_{ijk} is permutation symbol.

In addition, for a linear isotropic elastic material, the components of the corresponding work-conjugated stress tensors can be expressed as follows (Lam et al., 2003 [17])

$$\sigma_{ij} = 2\mu\varepsilon_{ij} + \lambda\varepsilon_{kk}\delta_{ij} \tag{7}$$

$$p_i = 2\mu l_0^2\,\gamma_i \tag{8}$$

$$\tau^{(1)}_{ijk} = 2\mu l_1^2\,\eta^{(1)}_{ijk} \tag{9}$$

$$m^s_{ij} = 2\mu l_2^2\,\chi^s_{ij} \tag{10}$$

where σ_{ij} is Cauchy force stress tensor, p_{ij} and $\tau^{(1)}_{ijk}$ are higher-order material stress tensors, and m^s_{ij} is couple stress tensor. Also, the parameters λ, μ and l_i $(i = 0, 1, 2)$ are called the Lame constants and the material length scale

parameters of the micro beam, respectively. The Lame constants λ and μ can also be determined with respect to Young's modulus E and the Poisson's ratio ϑ as $\lambda = \vartheta E/(1+\vartheta)(1-2\vartheta)$ and $\mu = E/2(1+\vartheta)$, respectively.

Governing Equations

The governing equations of motion and corresponding boundary conditions of a cracked micro cantilever beam based on the MSGT with using Dirac delta function are derived in this section. According to Fig. 1, with consideration of the Euler-Bernoulli beam theory, if the u_1, u_2 and u_3 denote the components of displacement vector along the x, y, and z axes, respectively, the displacement field in the linear-elastic micro beam can be written as follows

$$u_1 = u(x,t) - z\frac{\partial w(x,t)}{\partial x}\ ,\ u_2 = 0\ ,\ u_3 = w(x,t) \qquad (11)$$

where $u(x,t)$ and $w(x,t)$ are the axial displacement and the lateral deflection of the midline of the micro cantilever beam at any point x along the length of the micro beam in the x and z directions, respectively. Also, the $\frac{\partial w}{\partial x}$ stands for the angle of rotation about y-axis of the micro beam cross-section.

It is noted that the parameter z presents the distance of a point on the micro beam section with respect to the axis parallel of y-direction, passing through the micro beam centroid. By assuming small slops in the micro beam after deformation and substituting of Eq. (11) into Eqs. (2) – (6), the non-zero components of the strain tensor, the dilation gradient vector, the deviatoric stretch gradient tensor, the stress tensor, and the higher order stress tensor can be derived as follows

$$\varepsilon_{xx} = \frac{\partial u}{\partial x} - z\frac{\partial^2 w}{\partial x^2} \qquad (12)$$

$$\gamma_1 = \frac{\partial^2 u}{\partial x^2} - z\frac{\partial^3 w}{\partial x^3}\quad ,\quad \gamma_3 = -\frac{\partial^2 w}{\partial x^2} \qquad (13)$$

$$\begin{aligned}
&\eta^{(1)}_{111} = \frac{2}{5}\left(\frac{\partial^2 u}{\partial x^2} - z\frac{\partial^3 w}{\partial x^3}\right)\\
&\eta^{(1)}_{113} = \eta^{(1)}_{311} = \eta^{(1)}_{131} = \frac{-4}{15}\left(\frac{\partial^2 w}{\partial x^2}\right)\\
&\eta^{(1)}_{122} = \eta^{(1)}_{133} = \eta^{(1)}_{212} = \eta^{(1)}_{221} = \eta^{(1)}_{313} = \eta^{(1)}_{331}\\
&\qquad = \frac{1}{5}\left(-\frac{\partial^2 u}{\partial x^2} + z\frac{\partial^3 w}{\partial x^3}\right)\\
&\eta^{(1)}_{223} = \eta^{(1)}_{232} = \eta^{(1)}_{322} = \frac{1}{15}\left(\frac{\partial^2 w}{\partial x^2}\right)\\
&\eta^{(1)}_{333} = \frac{1}{5}\left(\frac{\partial^2 w}{\partial x^2}\right)
\end{aligned} \qquad (14)$$

$$\chi^s_{12} = \chi^s_{21} = -\frac{1}{2}\frac{\partial^2 w}{\partial x^2} \qquad (15)$$

Also, the nonzero components of Cauchy stress tensor and the higher-order stress tensor can be determined as follows

$$\sigma_{xx} = E\left(\frac{\partial u}{\partial x} - z\frac{\partial^2 w}{\partial x^2}\right) \qquad (16)$$

$$p_1 = 2\mu l_0^2\left(\frac{\partial^2 u}{\partial x^2} - z\frac{\partial^3 w}{\partial x^3}\right)\ ,\qquad p_1 = -2\mu l_0^2\left(\frac{\partial^2 w}{\partial x^2}\right) \qquad (17)$$

$$\begin{aligned}
&\tau^{(1)}_{111} = \frac{-4}{5}\mu l_1^2\left(\frac{\partial^2 u}{\partial x^2} - z\frac{\partial^3 w}{\partial x^3}\right)\\
&\tau^{(1)}_{113} = \tau^{(1)}_{311} = \tau^{(1)}_{131} = \frac{-8}{15}\mu l_1^2\left(\frac{\partial^2 w}{\partial x^2}\right)\\
&\tau^{(1)}_{122} = \tau^{(1)}_{133} = \tau^{(1)}_{212} = \tau^{(1)}_{221} = \tau^{(1)}_{313} = \tau^{(1)}_{331}\\
&\qquad = \frac{2}{5}\mu l_1^2\left(-\frac{\partial^2 u}{\partial x^2} + z\frac{\partial^3 w}{\partial x^3}\right)\\
&\tau^{(1)}_{223} = \tau^{(1)}_{232} = \tau^{(1)}_{322} = \frac{2}{15}\mu l_1^2\left(\frac{\partial^2 w}{\partial x^2}\right)\\
&\tau^{(1)}_{333} = \frac{2}{5}\mu l_1^2\left(\frac{\partial^2 w}{\partial x^2}\right)
\end{aligned} \qquad (18)$$

$$m^s_{12} = m^s_{21} = -\mu l_2^2\left(\frac{\partial^2 w}{\partial x^2}\right) \qquad (19)$$

Therefore, for a uniform micro cantilever beam without any crack, the strain energy of the system without considering the effect of axial load P, can be written as follows

$$\begin{aligned}
\pi_1 &= \frac{1}{2}\int_V \left(\sigma_{ij}\varepsilon_{ij} + p_i\,\gamma_i + \tau^{(1)}_{ijk}\,\eta^{(1)}_{ijk} + m^s_{ij}\,\chi^s_{ij}\right)dV\\
&= \frac{1}{2}\int_0^L \int_A \Bigg\{\Big[Ez^2\\
&\quad + \mu\left(2l_0^2 + \frac{8}{15}l_1^2 + l_2^2\right)\Big]\left(\frac{\partial^2 w}{\partial x^2}\right)^2\\
&\quad + \left[\mu z^2\left(2l_0^2 + \frac{4}{5}l_1^2\right)\right]\left(\frac{\partial^3 w}{\partial x^3}\right)^2\\
&\quad + EA\left(\frac{\partial u}{\partial x}\right)\\
&\quad + \mu A\Big(2l_0^2\\
&\quad + \frac{4}{5}l_1^2\Big)\left(\frac{\partial^2 u}{\partial x^2} - z\frac{\partial^3 w}{\partial x^3}\right)^2\Bigg\}dA\,dx
\end{aligned} \qquad (20)$$

where V denote the volume. By simplifying the Eq. (20), and also consider an open edge crack located at a distance L_c from the left end of the micro cantilever beam, the strain energy of the system with considering the effect of axial load P, can be determined as follows

$$\pi = \frac{1}{2}\int_0^L \Bigg\{ Q_1 \left(\frac{\partial^2 w}{\partial x^2}\right)^2 + Q_1 N_1 \left(\frac{\partial^3 w}{\partial x^3}\right)^2 + Q_2 \left(\frac{\partial u}{\partial x}\right)^2 + Q_2 N_1 \left(\frac{\partial^2 u}{\partial x^2}\right)^2 + Q_2 N_2 \left(\frac{\partial^2 w}{\partial x^2}\right)^2 + \delta(x - L_c) \Bigg[\eta_1 \, Q_1 \left(\frac{\partial^2 w}{\partial x^2}\right)^2 + \eta_1 \, Q_1 N_1 \left(\frac{\partial^3 w}{\partial x^3}\right)^2 + \eta_2 \, Q_2 \left(\frac{\partial u}{\partial x}\right)^2 + \eta_2 \, Q_2 N_1 \left(\frac{\partial^2 u}{\partial x^2}\right)^2 + \eta_2 \, Q_2 N_2 \left(\frac{\partial^2 w}{\partial x^2}\right)^2 \Bigg] \left(\frac{L - L_c}{2}\right) \Bigg\} dx + \frac{1}{2}\int_0^L P \left[2\left(\frac{\partial u}{\partial x}\right) + \left(\frac{\partial w}{\partial x}\right)^2 \right] dx \tag{21}$$

where

$$\begin{aligned} N_1 &= \frac{1}{2(1+\vartheta)}\left(2l_0^2 + \frac{4}{5}l_1^2\right) \\ N_2 &= \frac{1}{2(1+\vartheta)}\left(2l_0^2 + \frac{8}{15}l_1^2 + l_2^2\right) \\ Q_1 &= EI_b \\ Q_2 &= EA \end{aligned} \tag{22}$$

where $\delta(x)$ is Dirac delta function, $I_b = \int_A z^2 \, dA$ is the second moment of cross-section area of the micro beam about y-axis, and the coefficients η_1 and η_2 show reducing of cross-section area and second moment of cross-section area of the micro cantilever beam in crack location L_c , respectively. It is noted that the second moment of cross-section area for a uniform micro beam with rectangular cross section width b, height h, is $I_b = \frac{bh^3}{12} = \frac{Ah^2}{12}$, therefore the Eq. (22) can be written as follows

$$\begin{aligned} Q_1 N_1 &= \frac{EI_b h^2}{2(1+\vartheta)}\left[2\left(\frac{l_0}{h}\right)^2 + \frac{4}{5}\left(\frac{l_1}{h}\right)^2\right] \\ Q_2 N_1 &= \frac{6\,EI_b}{(1+\vartheta)}\left[2\left(\frac{l_0}{h}\right)^2 + \frac{4}{5}\left(\frac{l_1}{h}\right)^2\right] \\ Q_2 N_2 &= \frac{6\,EI_b}{(1+\vartheta)}\left[2\left(\frac{l_0}{h}\right)^2 + \frac{8}{15}\left(\frac{l_1}{h}\right)^2 + \left(\frac{l_2}{h}\right)^2\right] \end{aligned} \tag{23}$$

where l_0 , l_1, and l_2 are the material length scale parameters which is dependent on material property and can be determined experimentally by some typical standard tests such as the micro-bend and micro-torsion. For example, the material length scale parameters of nickel and epoxy have been determined to be $5\,\mu m$, and $17.6\mu m$, respectively (Fleck et al., 1994 [16]; Lam et al., 2003 [17]).

According to the above equations, It can be seen clearly that in the special case $l_0 = l_1 = l_2 = 0$, the obtaining natural frequency from governing equations is approached to the natural frequency values of a micro cantilever beam which is modeled based on the classical theory. In addition, when letting $l_0 = l_1 = 0$, the equations of micro cantilever beam are simplified to governing equations of the micro cantilever beam which is modeled based on the MCST.

The kinetic energy of the system T can also be obtained as follows

$$T = T_b + T_M \tag{24}$$

where the T_b and T_M are the kinetic energies of the micro cantilever beam and the kinetic energy of the concentrated mass which mounted at the free end of the micro beam, respectively. Also, we have

$$\begin{aligned} T_b &= \frac{1}{2}\int_0^L \rho A \, \dot{\vec{r}} . \dot{\vec{r}} \, dx + \frac{1}{2}\int_0^L \rho I_b \left(\frac{\partial \dot{w}}{\partial x}\right)^2 dx \\ \dot{\vec{r}} &= \dot{u}\boldsymbol{i} + \dot{w}\boldsymbol{k} \end{aligned} \tag{25}$$

where the $\dot{\vec{r}}$ is velocity vector of any particle. After substituting and to have some simplification, and also to consider the kinetic energy of the concentrated mass M, the Eq. (24) can be rewritten as follows

$$T = \frac{1}{2}\int_0^L \left[\rho A(\dot{u}^2 + \dot{w}^2) + \rho I_b \left(\frac{\partial \dot{w}}{\partial x}\right)^2\right] dx + \frac{1}{2}\int_0^L \delta(x - L)\left[M(\dot{u}^2 + \dot{w}^2) + I_M \left(\frac{\partial \dot{w}}{\partial x}\right)^2\right] dx \tag{26}$$

where $\delta(x)$ is Dirac delta function, and M and I_M are the concentrated mass and the mass moment of inertia of the concentrated mass M which mounted at the free end of the micro beam, respectively.

Now, Hamilton's principle is considered to derive of governing equations of motion of the system as follows

$$\int_{t_1}^{t_2} \delta(T - \pi + W)\, dt = 0 \tag{27}$$

where δT, $\delta\pi$ and δW are virtual variation of the kinetic energy, virtual variation of the strain energy, and virtual work done by external non-conservative forces on the system, respectively. For the presented system without external forces, the δW is equal zero.

By substituting the Eq. (21) and (26) into (27), and then using variational calculus, governing equations of lateral vibrations of the micro cantilever beam can be obtained as follows

$$
\begin{aligned}
&(Q_1 + Q_2N_2)\ \frac{\partial^4 w}{\partial x^4} - Q_1N_1\frac{\partial^6 w}{\partial x^6} \\
&+ (\eta_1Q_1 + \eta_2Q_2N_2)\left(\frac{L-L_c}{2}\right)\left\{\frac{\partial^2[\delta(x-L_c)]}{\partial x^2}\ \frac{\partial^2 w}{\partial x^2}\right. \\
&\left.+ 2\ \frac{\partial\ [\delta(x-L_c)]}{\partial x}\ \frac{\partial^3 w}{\partial x^3} + \delta(x-L_c)\ \frac{\partial^4 w}{\partial x^4}\right\} \\
&- \eta_1Q_1N_1\left(\frac{L-L_c}{2}\right)\left\{\frac{\partial^3[\delta(x-L_c)]}{\partial x^3}\ \frac{\partial^3 w}{\partial x^3}\right. \\
&+ 3\ \frac{\partial^2\ [\delta(x-L_c)]}{\partial x^2}\ \frac{\partial^4 w}{\partial x^4} + 3\ \frac{\partial\ [\delta(x-L_c)]}{\partial x}\ \frac{\partial^5 w}{\partial x^5} \\
&\left.+ \delta(x-L_c)\ \frac{\partial^6 w}{\partial x^6}\right\} - \frac{\partial}{\partial x}\left[P\ \frac{\partial\ w}{\partial x}\right] \\
&+ [\rho A + M\ \delta(x-L)]\ \ddot{w}\ - \rho I_b\frac{\partial^2 \ddot{w}}{\partial x^2} \\
&- I_M\left\{\frac{\partial[\delta(x-L)]}{\partial x}\ \frac{\partial \ddot{w}}{\partial x} + \delta(x-L)\frac{\partial^2 \ddot{w}}{\partial x^2}\right\} = 0
\end{aligned}
\tag{28}
$$

In the above equation, I_M, and P denote the mass moment of inertia of concentrated mass M, and the axial load, respectively.

Eq. (28) presents nonlinear partial differential governing equation of lateral vibrations of the micro cantilever beam subjected to an axial load, based on the MSGT with using Dirac delta function. Also, the classical and non-classical boundary conditions at each end of the micro cantilever beam can be written as follows

$$
\begin{aligned}
&w(0,t) = \frac{\partial w}{\partial x}(0,t) = 0 \\
&Q_1N_1\frac{\partial^3 w}{\partial x^3}(0,t) = 0
\end{aligned}
\tag{29}
$$

$$
\begin{aligned}
&-(Q_1 + Q_2N_2)\frac{\partial^3 w}{\partial x^3}(L^+,t) + Q_1N_1\frac{\partial^5 w}{\partial x^5}(L^+,t) \\
&\qquad + P\frac{\partial w}{\partial x}(L^+,t) = 0 \\
&(Q_1 + Q_2N_2)\frac{\partial^2 w}{\partial x^2}(L^+,t) - Q_1N_1\frac{\partial^4 w}{\partial x^4}(L^+,t) = 0 \\
&\frac{\partial^2 w}{\partial x^2}(L^+,t) = 0
\end{aligned}
\tag{30}
$$

where L^+ is the length of the micro cantilever beam plus a virtual length on the right side of the concentrated mass M.

Analytical Solution of the Governing Equation

In this section, the solution of Eq. (28) with its boundary conditions in Eqs. (29) and (30) are considered. To solve the governing equation (28), the assumed modes method is employed. The assumed modes method is closely tied to the Rayleigh-Ritz method. Actually, the discrete model obtained with the assumed modes method is exactly the same as the one obtained with the Rayleigh-Ritz method. The main difference between the two methods is that the Rayleigh-Ritz method is commonly used to solve the eigenvalue problem, while the assumed modes method is generally used to solve the vibration problem. In the assumed modes method, the solution of the vibration problem of the continuous system is assumed to be a series made up of a linear combination of admissible functions ψ_m (functions of the spatial coordinates) multiplied by time-dependent generalized coordinates W_m (t). Hence, for a one-dimensional continuous system, the assumed displacement solution is

$$
w(x,t) = \sum_{m=1}^{\infty}\psi_m(x)\ W_m\ (t) \tag{31}
$$

Where ψ_m are known shape functions that satisfy the admissible geometric boundary conditions of the system and also the $W_m(t)$ are time-dependent. The shape functions $\psi_m(x) = 1 - cos\left(\frac{m\pi x}{2L}\right)$, with $m = 1, 2, 3, \ldots$, are used to study of lateral vibrations of the cracked micro cantilever beam with boundary conditions Eqs. (29) and (30).

By substituting Eq. (31) into (28), and multiplying the results by orthogonal related modes $\psi_n(x)$ (with n is an arbitrary natural number), and then taking integration over the micro cantilever beam length, the obtaining result can be written as follows:

$$
\begin{aligned}
&\int_0^L \sum_{m=1}^{\infty}\left\{\begin{bmatrix}(Q_1 + Q_2N_2)\left(\frac{m\pi}{2L}\right)^4 \\ +Q_1N_1\left(\frac{m\pi}{2L}\right)^6 + P\left(\frac{m\pi}{2L}\right)^2\end{bmatrix} W_m\ cos\left(\frac{m\pi x}{2L}\right)\ cos\left(\frac{n\pi x}{2L}\right)\right. \\
&- (\eta_1Q_1 + \eta_2Q_2N_2)\left(\frac{L-L_c}{2}\right)\left\{\frac{\partial^2[\delta(x-L_c)]}{\partial x^2}\ \left(\frac{m\pi}{2L}\right)^2\right. \\
&\left.+ \delta(x-L_c)\ \left(\frac{m\pi}{2L}\right)^4\right\} W_m\ cos\left(\frac{m\pi x}{2L}\right)\ cos\left(\frac{n\pi x}{2L}\right) \\
&+ 2(\eta_1Q_1 \\
&+ \eta_2Q_2N_2)\left(\frac{L-L_c}{2}\right)\left\{\frac{\partial\ [\delta(x-L_c)]}{\partial x}\ \left(\frac{m\pi}{2L}\right)^3\right\} W_m\ sin\left(\frac{m\pi x}{2L}\right)\ cos\left(\frac{n\pi x}{2L}\right) \\
&+ \eta_1Q_1N_1\left(\frac{L-L_c}{2}\right)\left\{-\frac{\partial^3[\delta(x-L_c)]}{\partial x^3}\ \left(\frac{m\pi}{2L}\right)^3\right. \\
&\left.+ 3\ \frac{\partial\ [\delta(x-L_c)]}{\partial x}\ \left(\frac{m\pi}{2L}\right)^5\right\} W_m\ sin\left(\frac{m\pi x}{2L}\right)\ cos\left(\frac{n\pi x}{2L}\right) \\
&+ \eta_1Q_1N_1\left(\frac{L-L_c}{2}\right)\left\{-3\ \frac{\partial^2\ [\delta(x-L_c)]}{\partial x^2}\ \left(\frac{m\pi}{2L}\right)^4\right. \\
&\left.+ \delta(x-L_c)\ \left(\frac{m\pi}{2L}\right)^6\right\} W_m\ cos\left(\frac{m\pi x}{2L}\right)\ cos\left(\frac{n\pi x}{2L}\right) \\
&+ [\rho A + M\ \delta(x-L)]\ddot{W}_m\left(1 - cos\left(\frac{m\pi x}{2L}\right)\right)\left(1 - cos\left(\frac{n\pi x}{2L}\right)\right) \\
&+ \rho I_b\left(\frac{m\pi}{2L}\right)^2\ddot{W}_m\ cos\left(\frac{m\pi x}{2L}\right)\ cos\left(\frac{n\pi x}{2L}\right) \\
&+ I_M\left[\frac{\partial\ \delta(x-L)}{\partial x}\ \left(\frac{m\pi}{2L}\right)\right]\ddot{W}_m\ sin\left(\frac{m\pi x}{2L}\right)\ cos\left(\frac{n\pi x}{2L}\right) \\
&\left.+ I_M\left[\ \delta(x-L)\ \left(\frac{m\pi}{2L}\right)^2\right]\ddot{W}_m\ cos\left(\frac{m\pi x}{2L}\right)\ cos\left(\frac{n\pi x}{2L}\right)\right\} dx = 0
\end{aligned}
\tag{32}
$$

The following set of infinite ordinary differential equations can be obtained by calculating the integrals of Eqs. (32), for $n = 1, 2, 3, \ldots$:

$$\frac{L}{2}\left[(Q_1+Q_2N_2)\left(\frac{n\pi}{2L}\right)^4+Q_1N_1\left(\frac{n\pi}{2L}\right)^6+P\left(\frac{n\pi}{2L}\right)^2\right]W_n$$
$$+\sum_{m=1}^{\infty}\left\{(\eta_1Q_1+\eta_2Q_2N_2)\left(\frac{L-L_c}{2}\right)\left[\left(\frac{m\pi}{2L}\right)^4D_1\right.\right.$$
$$-\left(\frac{m\pi}{2L}\right)^2D_2+2\left(\frac{m\pi}{2L}\right)^3D_3\Big]$$
$$+(\eta_1Q_1N_1)\left(\frac{L-L_c}{2}\right)\left[3\left(\frac{m\pi}{2L}\right)^5D_3-\left(\frac{m\pi}{2L}\right)^3D_4\right.$$
$$\left.+\left(\frac{m\pi}{2L}\right)^6D_1-3\left(\frac{m\pi}{2L}\right)^4D_2\right]\Big\}W_m$$
$$+\sum_{m=1}^{\infty}\left\{\rho AL\left[\frac{3}{2}-\left(\frac{2}{n\pi}\right)sin\left(\frac{n\pi}{2}\right)-\left(\frac{2}{m\pi}\right)sin\left(\frac{m\pi}{2}\right)\right]\right.$$
$$+\left[\frac{\rho I_bL}{2}\left(\frac{n\pi}{2L}\right)^2\right]\ddot{W}_n$$
$$+M\left[1-cos\left(\frac{n\pi}{2}\right)-cos\left(\frac{m\pi}{2}\right)\right.$$
$$\left.+cos\left(\frac{m\pi}{2}\right)cos\left(\frac{n\pi}{2}\right)\right]$$
$$\left.+I_M\left[\left(\frac{m\pi}{2L}\right)\left(\frac{n\pi}{2L}\right)sin\left(\frac{m\pi}{2}\right)sin\left(\frac{n\pi}{2}\right)\right]\right\}\ddot{W}_m=0 \quad (33)$$

where

$$D_1=cos\left(\frac{m\pi L_c}{2L}\right)cos\left(\frac{n\pi L_c}{2L}\right)$$
$$D_2=-\left(\frac{m\pi}{2L}\right)^2cos\left(\frac{m\pi L_c}{2L}\right)cos\left(\frac{n\pi L_c}{2L}\right)$$
$$+2\left(\frac{mn\pi^2}{4L^2}\right)sin\left(\frac{m\pi L_c}{2L}\right)sin\left(\frac{n\pi L_c}{2L}\right)$$
$$-\left(\frac{n\pi}{2L}\right)^2cos\left(\frac{m\pi L_c}{2L}\right)cos\left(\frac{n\pi L_c}{2L}\right)$$
$$D_3=-\left(\frac{m\pi}{2L}\right)cos\left(\frac{m\pi L_c}{2L}\right)cos\left(\frac{n\pi L_c}{2L}\right)$$
$$+\left(\frac{n\pi}{2L}\right)sin\left(\frac{m\pi L_c}{2L}\right)sin\left(\frac{n\pi L_c}{2L}\right)$$
$$D_4=\left(\frac{m\pi}{2L}\right)^3cos\left(\frac{m\pi L_c}{2L}\right)cos\left(\frac{n\pi L_c}{2L}\right)$$
$$-\left(\frac{m\pi}{2L}\right)^2\left(\frac{n\pi}{2L}\right)sin\left(\frac{m\pi L_c}{2L}\right)sin\left(\frac{n\pi L_c}{2L}\right)$$
$$-2\left(\frac{m^2n\pi^3}{8L^3}\right)sin\left(\frac{m\pi L_c}{2L}\right)sin\left(\frac{n\pi L_c}{2L}\right)$$
$$+2\left(\frac{m\,n^2\pi^3}{8L^3}\right)cos\left(\frac{m\pi L_c}{2L}\right)cos\left(\frac{n\pi L_c}{2L}\right)$$
$$+\left(\frac{n\pi}{2L}\right)^2\left(\frac{m\pi}{2L}\right)cos\left(\frac{m\pi L_c}{2L}\right)cos\left(\frac{n\pi L_c}{2L}\right)$$
$$-\left(\frac{n\pi}{2L}\right)^3sin\left(\frac{m\pi L_c}{2L}\right)sin\left(\frac{n\pi L_c}{2L}\right) \quad (34)$$

Now, from the above equation, we can calculate the natural frequencies of the system approximately. Therefore, for this proposed, for $n=1$ and 2, and with using linearization, the Eq. (33) can be rewritten as follows

$$H_1\ddot{W}_n+H_2W_n=0 \quad (35)$$

where

$$H_1=\rho AL\left[\frac{3}{2}-2\left(\frac{2}{n\pi}\right)sin\left(\frac{n\pi}{2}\right)\right]+\left[\frac{\rho I_bL}{2}\left(\frac{n\pi}{2L}\right)^2\right]$$
$$+M\left[1-2\,cos\left(\frac{n\pi}{2}\right)+cos^2\left(\frac{n\pi}{2}\right)\right]$$
$$+I_M\left[\left(\frac{n\pi}{2L}\right)^2sin^2\left(\frac{n\pi}{2}\right)\right]$$
$$H_2=\frac{L}{2}\left[(Q_1+Q_2N_2)\left(\frac{n\pi}{2L}\right)^4+Q_1N_1\left(\frac{n\pi}{2L}\right)^6+P\left(\frac{n\pi}{2L}\right)^2\right]$$
$$+(\eta_1Q_1+\eta_2Q_2N_2)\left(\frac{L-L_c}{2}\right)\left[\left(\frac{n\pi}{2L}\right)^4cos^2\left(\frac{n\pi L_c}{2L}\right)\right]$$
$$-(\eta_1Q_1N_1)\left(\frac{L-L_c}{2}\right)\left[\left(\frac{n\pi}{2L}\right)^6cos\left(\frac{n\pi L_c}{L}\right)\right] \quad (36)$$

From Eq. (35), the natural frequencies of the cracked micro cantilever beam can be determined analytically for $n=1,2$ as follows

$$\omega_n=\sqrt{\frac{H_2}{H_1}}\quad,\quad for\ n=1,2 \quad (37)$$

where the coefficients H_1 and H_2 have been calculated from the Eq. (36).

Calculating of Coefficients η_1 and η_2

In this section, the coefficients η_1 and η_2 for a cracked micro beam with rectangular cross section are determined. In fact, the coefficients η_1 and η_2 show the reducing of cross-section area and second moment of cross-section area of the micro cantilever beam when occurred open edge crack or any other defect or flaw in the micro cantilever beam at location L_c , respectively. For a micro cantilever beam an open edge crack with depth a located at a distance L_c from the left end, (see Fig. 2), the coefficients η_1 and η_2 can be derived as follows

$$\eta_1=\frac{\frac{b(h-a)^3}{12}}{\frac{bh^3}{12}}-1=(1-\eta)^3-1$$
$$\eta_2=\frac{b(h-a)}{bh}-1=-\eta \quad (38)$$

where

$$\eta=\frac{a}{h} \quad (39)$$

Noted that the dimensionless coefficient η can be varied between 0 to 1, for the non-cracked or thoroughly cracked cases, respectively.

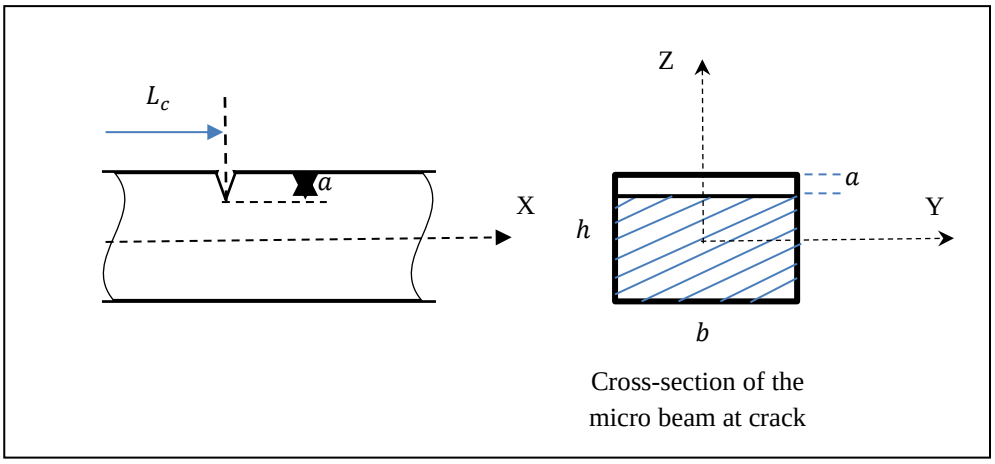

Fig. 2. Cross-section of the micro cantilever beam at open edge crack location

RESULTS AND DISCUSSION

The effect of size dependency on lateral vibrations behavior of a cracked micro cantilever beam subjected to an axial load and concentrated mass at its end free is studied in this section. In numerical analyses, it is assumed that the micro cantilever beam has been made of an epoxy material with the following mechanical properties (kahrobaiyan, et al., 2011 [38]): Young's modulus E = 1.44 GPa , Poison's ratio $\vartheta = 0.38$, density $\rho = 1220\, kg/m^3$. In addition, following data is considered for the micro cantilever beam: height $h = 20\, \mu m$, width $b = 2h$, length $L = 20h$, concentrated mass $M = 100 \times 10^{-6}\, gr$, rotary inertia of concentrated mass $I_M = 2.5 \times 10^{-9}\, (gr.mm^2)$.

First natural frequency of the cracked micro cantilever beam versus the open edge crack depth has been investigated in Fig. 3, for different values of the dimensionless material length parameters l_i/h (i=1, 2, 3), at the axial load $P = 0\, N$, the crack location $L_c = 0$, the concentrated mass $M = 100 \times 10^{-6}$ gr , the rotary inertia $I_M = 2.5 \times 10^{-9}\, (gr.mm^2)$, and $\frac{L}{h} = 20$. According to Figure 3, the natural frequency of the system decreases as the crack depth increases due to the decrease in stiffness. Additionally, based on this figure, the natural frequency increases with the increase of l_i/h. According to the relationship 37 and 36, as this ratio increases, the amount of H_2 increases, resulting in a higher natural frequency value. Also, according to the Fig. 3, it can be seen clearly when there is a thoroughly cracked at location $L_c = 0$, the fundamental frequency of the system is equal zero. This result match with the physical sense of the system.

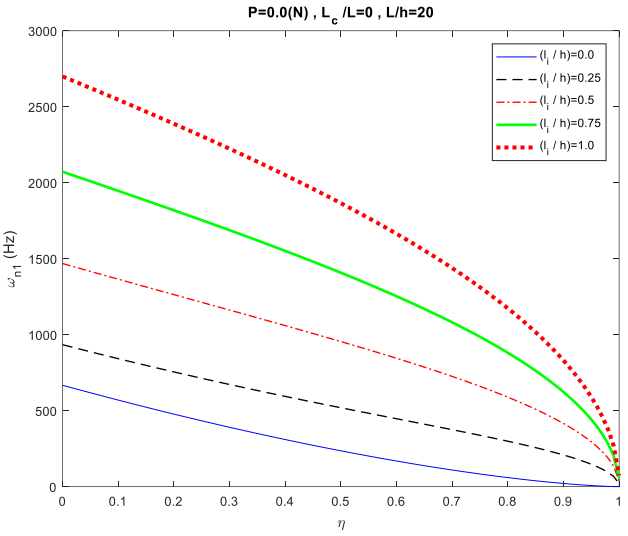

Fig. 3. Variation of the first natural frequency of the micro cantilever beam versus crack depth for different values of the $\boldsymbol{l_i/h}$ parameters

Variation of the fundamental natural frequency of the cracked micro cantilever beam versus the crack location L_c/L has been depicted in Fig. 4, for different dimensionless material length scale parameters $\frac{l_i}{h}(i = 0, 1, 2)$, at the axial load $P = 0$, and the crack depth $\eta = 0.4$. The obtained results indicate that as the material length scale parameters $\frac{l_i}{h}(i = 0, 1, 2)$ and crack location L_c increase, the value of the first natural frequency will also increase. When the crack is positioned further away from the end of the micro beam, the reduction in stiffness caused by the crack becomes less significant. As a result, the natural frequency increases with the greater distance between the crack and the beam's end. By increasing the material length scale parameters, while keeping other conditions unchanged, a notable observation is that the natural frequency of the system increases. For instance, when the values of the l_i/h is increased from 0 to

0.25, there is an approximate 40% increase in the natural frequency.

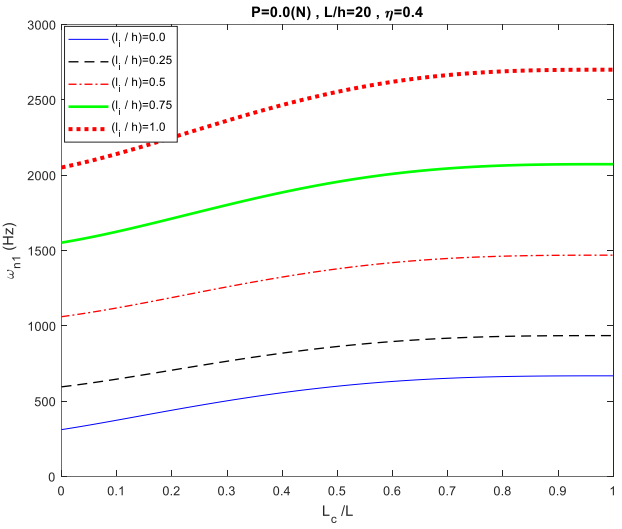

Fig. 4. Variation of first natural frequency of the micro cantilever beam versus crack location for different values of the $\boldsymbol{l_i/h}$ parameters and $\boldsymbol{\eta = 0.4}$

In addition, the second natural frequency of the cracked micro cantilever beam versus the crack location has been studied in Fig. 5, for different values of the dimensionless material length scale parameter l_i/h , the concentrated mass $M = 100 \times 10^{-6}$ gr, the rotary inertia $I_M = 2.5 \times 10^{-9}\ gr.mm^2$, the crack depth $\eta = 0.4$, and the axial load $P = 0\ N$.

The results show that the second natural frequency of the system will be increased by any increase of the dimensionless material length scale parameters $\frac{l_i}{h}(i = 0, 1, 2)$, but according to second mode shape of a cantilever beam, values of second natural frequency of the system can be increased or decreased with respect to the crack location on the micro cantilever beam. According to the graphs in Fig.5, the second natural frequency has a maximum point in different crack location. For example, at $\frac{l_i}{h} = 1$, the maximum value of the second natural frequency is at $\frac{L_c}{L} = 0.47$. The physical reason for the maximum points of the graph in Fig. 5 is the co-location of the node corresponding to the second mode shape and the crack. Because bending does not happen at the node of the second mode shape of the cantilever beam, and the existence of a crack at that point will not affect it. As a result, the crack at this point will not reduce the natural frequency.

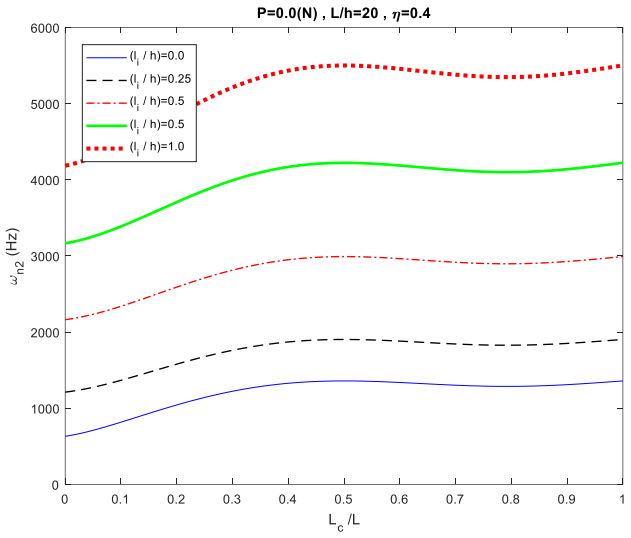

Fig. 5. Variation of second natural frequency of the micro cantilever beam versus crack location for different values of the $\boldsymbol{l_i/h}$ parameters and $\boldsymbol{\eta = 0.4}$

The first natural frequency of the cracked micro cantilever beam versus the crack location L_c/L has been presented in Fig. 6, for different values of the crack depth η, the dimensionless material length scale parameters $\frac{l_i}{h} = 1\ (i = 0, 1, 2)$, and $L/h = 20$. According to the results presented in Figure 6, it can be observed that the first natural frequency of the system decreases as the crack depth η increases. Additionally, when the crack is located closer to the fixed support of the cantilever beam, the first natural frequency is reduced. In other words, a deeper crack and proximity to the fixed support both lead to a decrease in the system's first natural frequency.

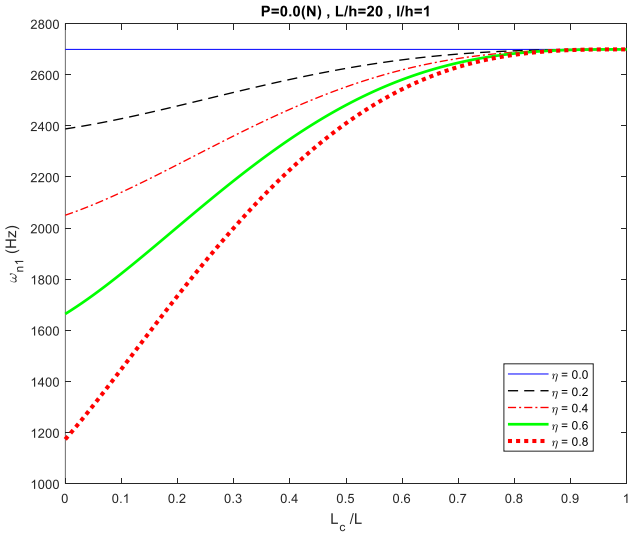

Fig. 6. Variation of first natural frequency of the micro cantilever beam versus crack location for different values of crack depth and $\boldsymbol{l_i/h = 1.0}$

Also, the second natural frequency behavior of the cracked micro cantilever beam versus the crack location L_c/L has been studied in Fig. 7, for different values of the crack depth η , $\frac{l_i}{h} = 1\ (i = 0, 1, 2)$, and $L/h = 20$. The results in Fig. 7 show the behavior of the second natural frequency of the system with respect to the crack depth η, and also the crack location L_c. This behavior corresponds to the physical sense and second mode shape of the system. The presence of maximum and minimum points in the graph of Fig. 7 has a physical reason. From the physical point of view, the second mode shape of a cantilever beam has one node. The graph in Fig. 7 is drawn based on the crack location. When the place of the crack is located on the node of the second mode shape, because the cantilever beam does not have bending at this point, as a result, the existence of a crack at this point will not affect the behavior of the cantilever beam. In the graph of Fig. 7, the maximum point is due to the location of the crack on the node of the second mode shape.

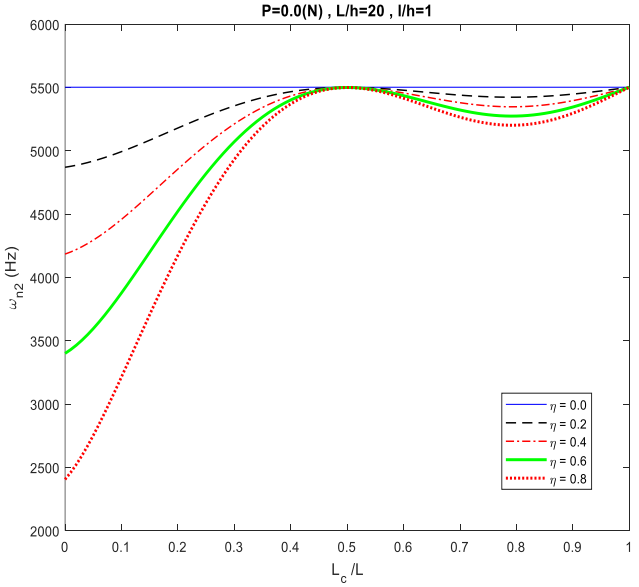

Fig. 7. Variation of second natural frequency of the micro cantilever beam versus crack location for different values of crack depth and $\boldsymbol{l_i/h = 1.0}$

Variation of the first natural frequency of the cracked micro cantilever beam versus the crack location L_c/L has been investigated in Fig. 8, for different values of the l_i/h parameters and $\eta = 0.4$, the axial load $P = 0$, and $L/h = 20$. It was mentioned that in the case of $l_i = 0$, the governing equation is the same as the governing equation of the micro cantilever beam based on the classical theory. Because the governing equations are the same as the classical equations, the natural frequencies will also be equal to the natural frequency of the micro cantilever beam with the governing equation based on the classical theory. In addition, when $l_0 = l_1 = 0$, the governing equation of lateral motion are simplified to a micro cantilever beam which modeled based on the MCST. Also, the results in Fig. 8 show that the fundamental natural frequency of the system will be decreased when the crack location is approached to fixed supported of the micro cantilever beam.

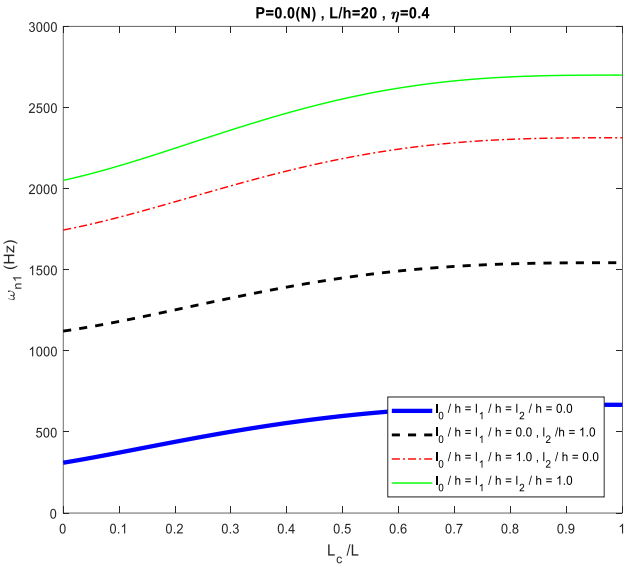

Fig. 8. Variation of first natural frequency of the micro cantilever beam versus crack location for different values of the $\boldsymbol{l_i/h}$ parameters and $\boldsymbol{\eta = 0.4}$

Effect of the axial load values P and also the dimensionless material length scale parameters l_i/h on the variation of the fundamental frequency of the cracked micro cantilever beam have been presented in Fig. 9, for crack location $L_c = 0$, and $\eta = 0.4$. It is noted that the negative values of axial load state that the axial load is in the compressive case. Based on the findings presented in Fig. 9, the numerical analysis reveals a clear trend: as the compressive axial load (P) increases, there is a notable decrease in the first natural frequency of the system. This phenomenon, commonly referred to as the buckling load, occurs when the first natural frequency approaches zero for the micro cantilevered beam. Understanding the implications of this trend is crucial for assessing the stability and structural behavior of micro cantilevered beams. By observing the relationship between the applied axial load and the first natural frequency, researchers gain insights into the critical buckling threshold. This knowledge plays a significant role in the design and optimization of microelectromechanical systems (MEMS) and related applications.

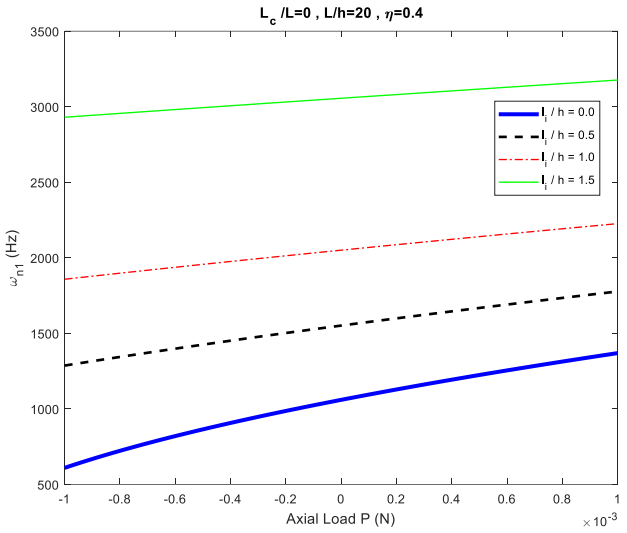

Fig. 9. Variation of first natural frequency of the micro cantilever beam versus axial load $\boldsymbol{P}$ for different values of the $\boldsymbol{l_i/h}$ parameters, crack location $\boldsymbol{L_c = 0}$, and $\boldsymbol{\eta = 0.4}$

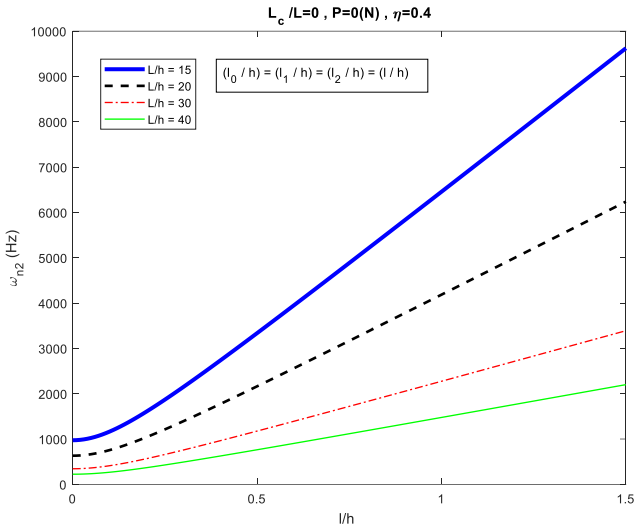

Fig. 11. Variation of second natural frequency of the micro cantilever beam versus the dimensionless material length scale parameter $\boldsymbol{l/h}$ for different values of micro beam length $\boldsymbol{L/h}$, crack location $\boldsymbol{L_c = 0}$, and $\boldsymbol{\eta = 0.4}$

Variation of first and second natural frequencies of the cracked micro cantilever beam versus the dimensionless material length scale parameter $\frac{l_i}{R}$ $(i = 0, 1, 2) = l/h$ have been depicted in Figs. 10 and 11, respectively, for different values of micro beam length L/h , crack location $L_c = 0$, crack depth $\eta = 0.4$, and axial load $P = 0$.

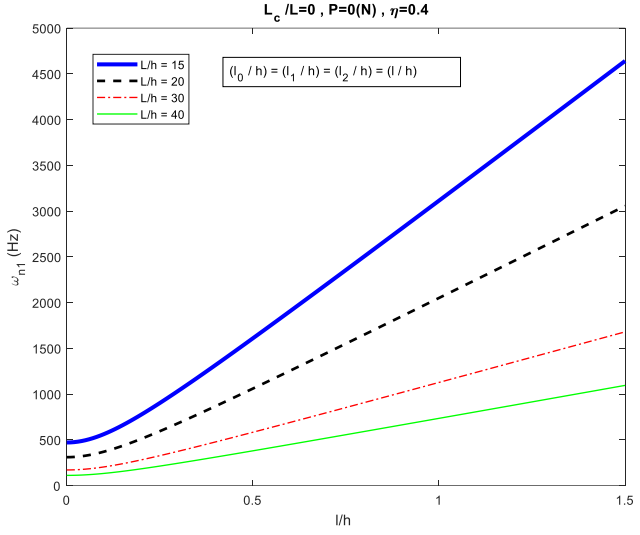

Fig. 10. Variation of first natural frequency of the micro cantilever beam versus the dimensionless material length scale parameter $\boldsymbol{l/h}$ for different values of micro beam length $\boldsymbol{L/h}$, crack location $\boldsymbol{L_c = 0}$, and $\boldsymbol{\eta = 0.4}$

Variation of the first natural frequency of the cracked micro cantilever beam versus the dimensionless material length scale parameters $\frac{l_i}{h}$ $(i = 0, 1, 2) = \frac{l}{h}$, have been depicted in Fig. 12, for different values of crack location L_c/h , at axial load $P = 0\ N$, crack depth and $\eta = 0.4$, and $\frac{L}{h} = 20$.

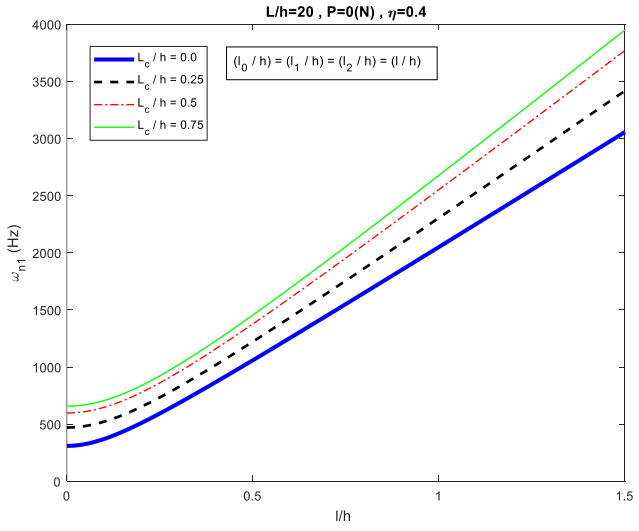

Fig. 12. Variation of first natural frequency of the micro cantilever beam versus the dimensionless material length scale parameter $\boldsymbol{l/h}$ for different values of crack location $\boldsymbol{L_c/h}$, and $\boldsymbol{\eta = 0.4}$

At final, the fundamental natural frequency of the cracked micro cantilever beam versus the concentrated mass M and rotary inertia I_M , has been presented in Fig. 13, for different values of the crack depth η, and crack location $L_c = 0$.

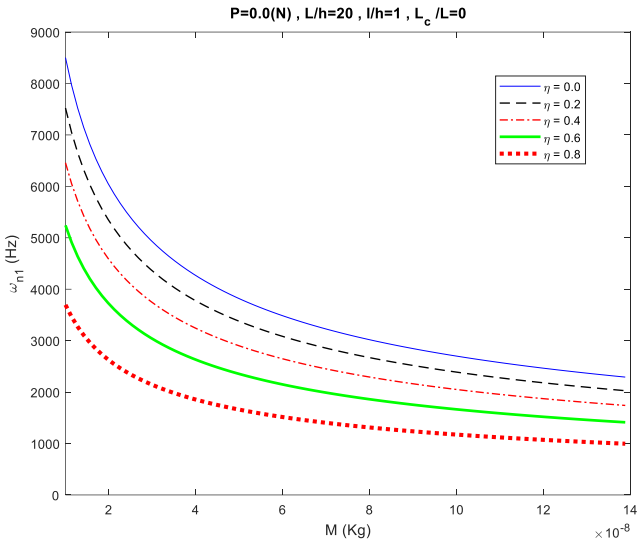

Fig. 13. Variation of first natural frequency of the micro cantilever beam versus concentrated mass $\boldsymbol{M}$, for different values of crack depth $\boldsymbol{\eta}$, and crack location $\boldsymbol{L_c = 0}$

Verification

The finite element method was employed to validate the analytical calculations in this study. A finite element simulation was conducted using Abacus software, focusing on a special case involving a zero material length scale parameters. The simulation result for the first mode is illustrated in Figure 14. By comparing these obtained findings with those in Figure 4, a comprehensive comparison is presented in Table 1. Importantly, the results of the finite element model and numerical simulation exhibit satisfactory convergence.

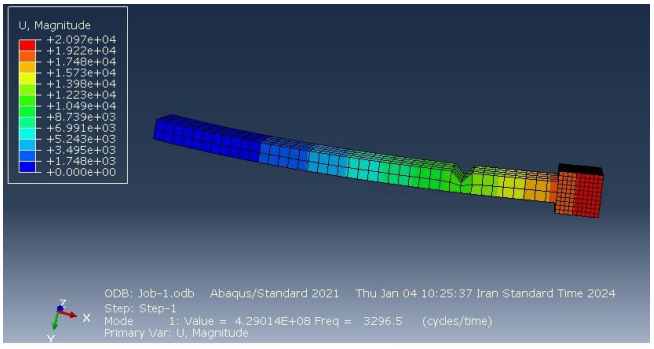

Fig. 14. Finite element model the open edge cracked micro cantilever beam for $\frac{l_i}{h} = \mathbf{0}$

Table 1. Comparison of finite element model and analysis results of open edge cracked micro cantilever beam for $\frac{l_i}{h} = \mathbf{0}$

L_c/L	$\omega_1(A)$	$\omega_1(FE)$	Error (%)
0.2	470	457	2.7
0.5	530	496	6.4
0.8	580	524	9.6

SUMMARY AND CONCLUSION

This study focuses on a cracked micro cantilever beam with a concentrated mass under axial load. It investigates the influence of size effects on the lateral vibrations of the micro beam. The governing equations of motion are derived using the non-classical theory of MSGT (modified strain gradient theory). The assumed modes approach is employed to transform the equations into a set of ordinary differential equations. Analytical calculations based on the MSGT are used to determine the first and second natural frequencies of the cracked micro cantilever beam. A simplified model for an open edge crack utilizing the Dirac delta function is proposed. To investigate the system's characteristics, numerical simulations were performed. These simulations specifically focused on exploring the natural frequencies of the system under various parameter values.

The results indicated several significant conclusions, including:

- The natural frequency of the system decreases as the crack depth increases due to the decrease in stiffness caused by the crack.
- The first natural frequency increases as the material length scale parameters (l_0/h, l_1/h, l_2/h) and crack location (Lc) increase. When the crack is positioned further away from the end of the micro beam, the reduction in stiffness caused by the crack becomes less significant, resulting in higher natural frequencies.
- The second natural frequency of the system can be increased or decreased depending on the crack location with respect to the second mode shape of the cantilever beam. If the crack is located at a node of the second mode shape where there is no bending, it does not significantly affect the behavior of the beam.

These findings provide insights into the behavior of micro cantilever beams with cracks and the impact of size effects. The study's results have practical implications for designing and analyzing such systems while considering crack position, depth, material length scale parameters, concentrated mass, axial load, and beam length.

REFERENCES

[1] Pei J, Tian F, Thundat T. Glucose biosensor based on the microcantilever. Analytical Chemistry. 2004 Jan 15;76(2):292-7.

[2] Lun FY, Zhang P, Gao FB, Jia HG. Design and fabrication of micro-optomechanical vibration sensor. Microfabrication Technology. 2006;120(1):61-4.

[3] McMahan LE, Castleman BW. Characterization of vibrating beam sensors during shock and vibration. InPLANS 2004. Position Location and Navigation Symposium (IEEE Cat. No. 04CH37556) 2004 Apr 26 (pp. 102-110). IEEE.

[4] Zhang YH, Ding G, Shun X, Gu D, Cai B, Lai Z. Preparing of a high speed bistable electromagnetic RF MEMS switch. Sensors and Actuators A: Physical. 2007 Mar 15;134(2):532-7.

[5] Coutu Jr RA, Kladitis PE, Starman LA, Reid JR. A comparison of micro-switch analytic, finite element, and experimental results. Sensors and Actuators A: Physical. 2004 Sep 21;115(2-3):252-8.
[6] Rezazadeh G, Tahmasebi A, Zubstov M. Application of piezoelectric layers in electrostatic MEM actuators: controlling of pull-in voltage. Microsystem technologies. 2006 Oct;12:1163-70.
[7] Zand MM, Ahmadian MT. Vibrational analysis of electrostatically actuated microstructures considering nonlinear effects. Communications in Nonlinear Science and Numerical Simulation. 2009 Apr 1;14(4):1664-78.
[8] Hu YC, Chang CM, Huang SC. Some design considerations on the electrostatically actuated microstructures. Sensors and Actuators A: Physical. 2004 Apr 15;112(1):155-61.
[9] Mojahedi M, Zand MM, Ahmadian MT. Static pull-in analysis of electrostatically actuated microbeams using homotopy perturbation method. Applied Mathematical Modelling. 2010 Apr 1;34(4):1032-41.
[10] Abdel-Rahman EM, Younis MI, Nayfeh AH. Characterization of the mechanical behavior of an electrically actuated microbeam. Journal of Micromechanics and Microengineering. 2002 Sep 5;12(6):759.
[11] Mahdavi MH, Farshidianfar A, Tahani M, Mahdavi S, Dalir H. A more comprehensive modeling of atomic force microscope cantilever. Ultramicroscopy. 2008 Dec 1;109(1):54-60.
[12] Chang WJ, Lee HL, Chen TY. Study of the sensitivity of the first four flexural modes of an AFM cantilever with a sidewall probe. Ultramicroscopy. 2008 Jun 1;108(7):619-24.
[13] Turner JA, Wiehn JS. Sensitivity of flexural and torsional vibration modes of atomic force microscope cantilevers to surface stiffness variations. Nanotechnology. 2001 Aug 28;12(3):322.
[14] Lee HL, Chang WJ. Coupled lateral bending–torsional vibration sensitivity of atomic force microscope cantilever. Ultramicroscopy. 2008 Jul 1;108(8):707-11.
[15] Lam DC, Chong AC. Indentation model and strain gradient plasticity law for glassy polymers. Journal of materials research. 1999 Sep;14(9):3784-8.
[16] Fleck NA, Muller GM, Ashby MF, Hutchinson JW. Strain gradient plasticity: theory and experiment. Acta Metallurgica et materialia. 1994 Feb 1;42(2):475-87.
[17] Lam DC, Yang F, Chong AC, Wang J, Tong P. Experiments and theory in strain gradient elasticity. Journal of the Mechanics and Physics of Solids. 2003 Aug 1;51(8):1477-508.
[18] Chong AC, Lam DC. Strain gradient plasticity effect in indentation hardness of polymers. Journal of Materials Research. 1999 Oct;14(10):4103-10.
[19] Eringen AC. Nonlocal polar elastic continua. International journal of engineering science. 1972 Jan 1;10(1):1-6.
[20] Mindlin RD, Tiersten H. Effects of couple-stresses in linear elasticity. Archive for Rational Mechanics and analysis. 1962 Jan 1;11(1):415-48.
[21] Yang FA, Chong AC, Lam DC, Tong P. Couple stress based strain gradient theory for elasticity. International journal of solids and structures. 2002 May 1;39(10):2731-43.
[22] Gurtin ME, Murdoch AI. Surface stress in solids. International journal of Solids and Structures. 1978 Jan 1;14(6):431-40.
[23] Mindlin RD. Second gradient of strain and surface-tension in linear elasticity. International journal of solids and structures. 1965 Nov 1;1(4):417-38.
[24] Mindlin RD, Eshel N. On first strain-gradient theories in linear elasticity. International Journal of Solids and Structures. 1968 Jan 1;4(1):109-24.
[25] Fleck NA, Hutchinson J. A phenomenological theory for strain gradient effects in plasticity. Journal of the Mechanics and Physics of Solids. 1993 Dec 1;41(12):1825-57.
[26] Park SK, Gao XL. Bernoulli–Euler beam model based on a modified couple stress theory. Journal of Micromechanics and Microengineering. 2006 Sep 15;16(11):2355.
[27] Ma HM, Gao XL, Reddy J. A microstructure-dependent Timoshenko beam model based on a modified couple stress theory. Journal of the Mechanics and Physics of Solids. 2008 Dec 1;56(12):3379-91.
[28] Liang LN, Ke LL, Wang YS, Yang J, Kitipornchai S. Flexural vibration of an atomic force microscope cantilever based on modified couple stress theory. International Journal of Structural Stability and Dynamics. 2015 Oct 16;15(07):1540025.
[29] Asghari M, Kahrobaiyan MH, Rahaeifard M, Ahmadian MT. Investigation of the size effects in Timoshenko beams based on the couple stress theory. Archive of Applied Mechanics. 2011 Jul;81:863-74.
[30] Ghiasi EK. Application of modified couple stress theory to study dynamic characteristics of electrostatically actuated micro-beams resting upon squeeze-film damping under mechanical shock. Int. J. Adv. Mater. Sci. Eng. 2016;6(1):1-5.
[31] Dai HL, Wang YK, Wang L. Nonlinear dynamics of cantilevered microbeams based on modified couple stress theory. International Journal of Engineering Science. 2015 Sep 1;94:103-12.
[32] Şimşek M, Aydın M. Size-dependent forced vibration of an imperfect functionally graded (FG) microplate with porosities subjected to a moving load using the modified couple stress theory. Composite Structures. 2017 Jan 15;160:408-21. doi: http://dx.doi.org/10.1016/j.compstruct.2016.10.034.

[33] Askari AR, Tahani M. Size-dependent dynamic pull-in analysis of geometric non-linear micro-plates based on the modified couple stress theory. Physica E: Low-dimensional Systems and Nanostructures. 2017 Feb 1;86:262-74. http://dx.doi.org/10.1016/j.physe.2016.10.035.

[34] Alinaghizadeh F, Shariati M, Fish J. Bending analysis of size-dependent functionally graded annular sector microplates based on the modified couple stress theory. Applied Mathematical Modelling. 2017 Apr 1;44:540-56. doi: 10.1016/j.apm.2017.02.018.

[35] Guo J, Chen J, Pan E. Free vibration of three-dimensional anisotropic layered composite nanoplates based on modified couple-stress theory. Physica E: Low-dimensional Systems and Nanostructures. 2017 Mar 1;87:98-106. http://dx.doi.org/10.1016/j.physe.2016.11.025.

[36] He D, Yang W, Chen W. A size-dependent composite laminated skew plate model based on a new modified couple stress theory. acta mechanica solida sinica. 2017 Feb 1;30(1):75-86.

[37] Vatankhah R, Kahrobaiyan MH, Alasty A, Ahmadian M. Nonlinear forced vibration of strain gradient microbeams. Applied Mathematical Modelling. 2013 Oct 1;37(18-19):8363-82.

[38] Kahrobaiyan MH, Asghari M, Rahaeifard M, Ahmadian M. A nonlinear strain gradient beam formulation. International Journal of Engineering Science. 2011 Nov 1;49(11):1256-67.

[39] Kahrobaiyan MH, Asghari M, Ahmadian MT. Strain gradient beam element. Finite Elements in Analysis and Design. 2013 Jun 1;68:63-75.

[40] Joseph RP, Wang BL, Samali B. Size effects on double cantilever beam fracture mechanics specimen based on strain gradient theory. Engineering Fracture Mechanics. 2017 Jan 1;169:309-20.

[41] Ansari R, Gholami R, Shojaei MF, Mohammadi V, Darabi MA. Coupled longitudinal-transverse-rotational free vibration of post-buckled functionally graded first-order shear deformable micro-and nano-beams based on the Mindlin's strain gradient theory. Applied Mathematical Modelling. 2016 Dec 1;40(23-24):9872-91. doi: 10.1016/j.apm.2016.06.042.

[42] Mirsalehi M, Azhari M, Amoushahi H. Buckling and free vibration of the FGM thin micro-plate based on the modified strain gradient theory and the spline finite strip method. European Journal of Mechanics-A/Solids. 2017 Jan 1;61:1-3.

[43] Ansari R, Gholami R, Shojaei MF, Mohammadi V, Sahmani S. Bending, buckling and free vibration analysis of size-dependent functionally graded circular/annular microplates based on the modified strain gradient elasticity theory. European Journal of Mechanics-A/Solids. 2015 Jan 1;49:251-67. doi: 10.1016/j.euromechsol.2014.07.014.

[44] Loya J, López-Puente J, Zaera R, Fernández-Sáez J. Free transverse vibrations of cracked nanobeams using a nonlocal elasticity model. Journal of Applied Physics. 2009 Feb 15;105(4).

[45] Tadi Beni Y, Jafaria A, Razavi H. Size effect on free transverse vibration of cracked nano-beams using couple stress theory. International Journal of Engineering-Transactions B: Applications, 2014;28(2):296.

[46] Hasheminejad SM, Gheshlaghi B, Mirzaei Y, Abbasion S. Free transverse vibrations of cracked nanobeams with surface effects. Thin Solid Films. 2011 Feb 1;519(8):2477-82.

[47] Wang K, Wang B. Timoshenko beam model for the vibration analysis of a cracked nanobeam with surface energy. Journal of Vibration and Control. 2015 Sep;21(12):2452-64.

[48] Torabi K, Dastgerdi JN. An analytical method for free vibration analysis of Timoshenko beam theory applied to cracked nanobeams using a nonlocal elasticity model. Thin Solid Films. 2012 Aug 31;520(21):6595-602.

[49] Liu SJ, Qi SH, Zhang WM. Vibration behavior of a cracked micro-cantilever beam under electrostatic excitation. Zhendong yu Chongji/Journal of Vibration and Shock. 2013;32(17):41-5.

[50] Akbaş ŞD. Free vibration of edge cracked functionally graded microscale beams based on the modified couple stress theory. International Journal of Structural Stability and Dynamics. 2017 Apr 31;17(03):1750033.

[51] Akbarzadeh Khorshidi M, Shaat M, Abdelkefi A, Shariati M. Nonlocal modeling and buckling features of cracked nanobeams with von Karman nonlinearity. Applied Physics A. 2017 Jan;123:1-2.

[52] Esen I, Özarpa C, Eltaher MA. Free vibration of a cracked FG microbeam embedded in an elastic matrix and exposed to magnetic field in a thermal environment. Composite Structures. 2021 Apr 1;261:113552.

[53] Darban H, Luciano R, Basista M. Free transverse vibrations of nanobeams with multiple cracks. International Journal of Engineering Science. 2022 Jul 1;177:103703.

[54] Thai CH, Ferreira AJ, Phung-Van P. Free vibration analysis of functionally graded anisotropic microplates using modified strain gradient theory. Engineering Analysis with Boundary Elements. 2020 Aug 1;117:284-98.